Extended document: A new robust methodology for the identification of parameters on the electrical response of photovoltaic systems through the application of polar coordinates

Carlos Cárdenas-Bravo[1], Sylvain Lespinats[2], and Denys Dutykh[3]

[1] *Univ. Grenoble Alpes, Univ. Savoie Mont Blanc, CNRS, LAMA, Chambéry, 73 000, France*
[2]*Univ. Grenoble Alpes, CEA, Liten, INES, Le Bourget du Lac, 73 375, France*
[3] *Mathematics Department, Khalifa University, Abu Dhabi, PO Box 127 788, United Arab Emirates*

Abstract

The present document extends the ideas presented in the poster and is organized into four sections. Section I introduces the single-diode model, highlighting its main characteristics. Section II presents the polar single-diode model. In Section III, the cost functions evaluated in this work are described. Finally, Section IV details the results obtained.

Nomenclature

Acronyms

NREL National Renewable Energy Laboratory

ODR Ortogonal distance regression

PV Photovoltaic

RMSD Root mean squared deviation

SDM Single-diode model

Abstract prepared to 2024 European PVPMC Workshop, Copenhagen, Denmark.

Variables

I	Electric current
P	Electric power
T	Temperature
V	Electric voltage

Physical constants

k_B	Boltzmann's constant ($1.380\,649 \times 10^{-23}\ \mathrm{J\,K^{-1}}$)
q	Elementary electric charge ($1.602\,176\,634 \times 10^{-19}\ \mathrm{C}$)

Subscripts

k	Estimated variable
m	Measured variable
mp	Maximum power
nf	Noise free
nn	Normally distributed noise
oc	Open-circuit
pv	Photovoltaic
sc	Short-circuit

Model parameters

G_sh	Shunt conductance
I_o	Dark saturation current of the diode
I_ph	Photo-generated current
R_s	Series resistance
A	Equivalent thermal voltage
n	Non-ideal factor of the diode

I. Single-diode model

The electrical response of any solar photovoltaic device can be represented as a current-voltage (I–V) curve, by using its photovoltaic voltage, V_{pv}, and photovoltaic current I_{pv}. From this I–V curve, three points can be extracted: the open-circuit point $(V_{\mathrm{oc}},\, 0)$, the short-circuit point $(0,\, I_{\mathrm{sc}})$, and the maximum power point $(V_{\mathrm{mp}},\, I_{\mathrm{mp}})$. In this work, these points are named as cardinal points. Fig. 1(a) shows the typical I–V curve measured in real operating conditions. In turn, the I–V curve can be scaled according to V_{oc} and I_{sc}:

$$\{v_{\mathrm{pv}},\, i_{\mathrm{pv}}\} \coloneqq \left\{\frac{V_{\mathrm{pv}}}{V_{\mathrm{oc}}},\, \frac{I_{\mathrm{pv}}}{I_{\mathrm{sc}}}\right\}, \tag{1}$$

where v_{pv} and i_{pv} represent the scaled versions of the photovoltaic voltage and the photovoltaic current, respectively. Fig. 1(b) depicts the scaled I–V curve.

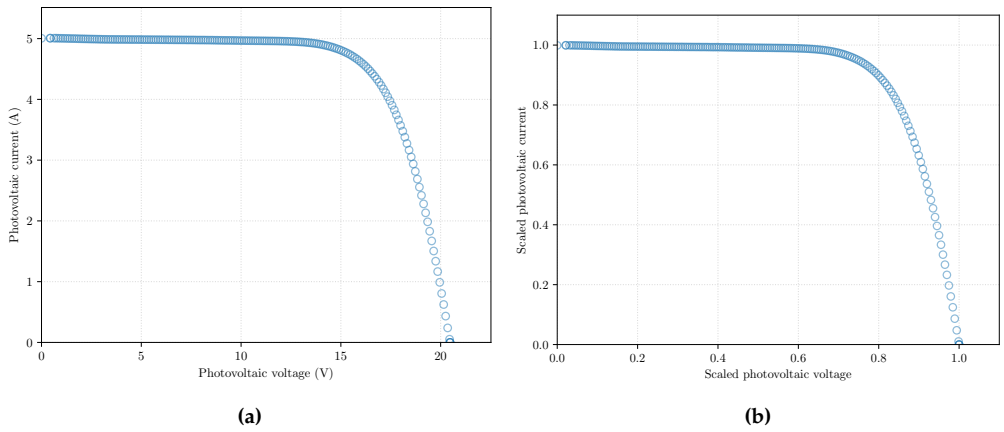

Fig. 1. Example I–V curve. Panel (a) shows the measured I–V curve, and panel (b) shows the scaled I–V curve. Data extracted from NREL dataset [1].

Remark 1. *In this work, all variables and parameters written in lowercase are assumed to be scaled.*

The single-diode model (SDM) is a model derived from the solar-state physics [2] which explains the main effects in the solar cell. This model is described by means of five parameters: the photo-generated current, I_{ph}, which takes into account the effect of the absorbed light by the solar cell; the dark saturation current of the diode, I_{o}, and the non-ideal factor of the diode n, both describing intrinsic characteristics of solar cell; the series resistance, R_{s}, incorporating external undersired resistances on the model such as the contact resistance; and

the shunt conductance, G_{sh}, which includes the effect of current leakage in the solar cell. Mathematically, the SDM is expressed as

$$f_{sd} = I_o \exp\left(\frac{q\left(V_{pv} + R_s I_{pv}\right)}{N_s n k_B T_{cell}}\right) + G_{sh}\left(V_{pv} + R_s I_{pv}\right) + I_{pv} - (I_{ph} + I_o), \tag{2}$$

where T_{cell} represents the cell temperature (measured in kelvin K), q is the elementary electrical charge, and k_B is the Boltzmann constant. For simplifying the nomenclature of the model, the equivalent thermal voltage A is incorporated into the formulation, defined as

$$A := \frac{N_s n k_B T_{cell}}{q}. \tag{3}$$

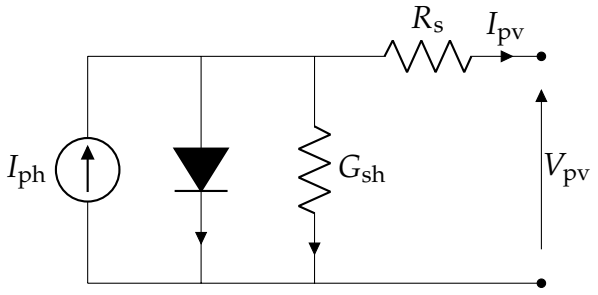

Fig. 2. Single-diode model's electrical diagram. This model is composed by five parameters distributed into four electrical elements: the current source (photo-generated current, I_{ph}), the diode (dark saturation current of the diode, I_o, and ideality factor, n, parameters), and two resistances (series resistance, R_s, and shunt resistance, R_{sh}, parameters). The small arrows indicates the reference of the current.

Another consideration on the SDM is that its parameters can be scaled according to V_{oc} and I_{sc}. Then, the I–V computed from the scaled SDM satisfy $0 \leqslant i_{pv} \leqslant 1$ and $0 \leqslant v_{pv} \leqslant 1$. The set of scaled parameters is computed as

$$\left\{i_{ph}\,, i_o,\, a,\, r_s,\, g_{sh}\right\} := \left\{\frac{I_{ph}}{I_{sc}}, \frac{I_o}{I_{sc}}, \frac{A}{V_{oc}}, \frac{I_{sc}R_s}{V_{oc}}, \frac{V_{oc}G_{sh}}{I_{sc}}\right\}. \tag{4}$$

The non-linearty of the SDM make difficult to identify the its five parameters given input measurements. For this, solutions such as expressing the SDM as function of one variables has been proposed [3, 4, 5]. This representation is known as the one-dimensional single-diode model (SDM-1), and incorporates into the formulation the cardinal points (see details in). Therefore, to identify the SDM-1 only one parameter has to be computed, simplifying the computation of the SDM. For this work, the SDM-1 is used as basis for all cost functions evaluated.

II. The polar single-diode model

The polar single-diode model was firstly introduced by S. Lespinats *et al.* [6]. In S. Lespinats procedure, the SDM is expressed making

$$V_{\mathrm{pv}} = V_{\mathrm{oc}} \rho \cos(\varphi), \tag{5}$$

$$I_{\mathrm{pv}} = I_{\mathrm{sc}} \rho \sin(\varphi), \tag{6}$$

where ρ represents the radius (dimensionless) and φ is the angle (measured in radians.) Then,

$$f_{\mathrm{polar}} \coloneqq i_{\mathrm{o}} \exp\left(\frac{\rho\left(\cos(\varphi) + r_{\mathrm{s}} \sin(\varphi)\right)}{a}\right) + g_{\mathrm{sh}} \rho \cos(\varphi) + (g_{\mathrm{sh}} r_{\mathrm{s}} + 1)\rho \sin(\varphi) - \left(i_{\mathrm{ph}} + i_{\mathrm{o}}\right). \tag{7}$$

This representation is called polar SDM, and graphically is depicted by Fig. 3.

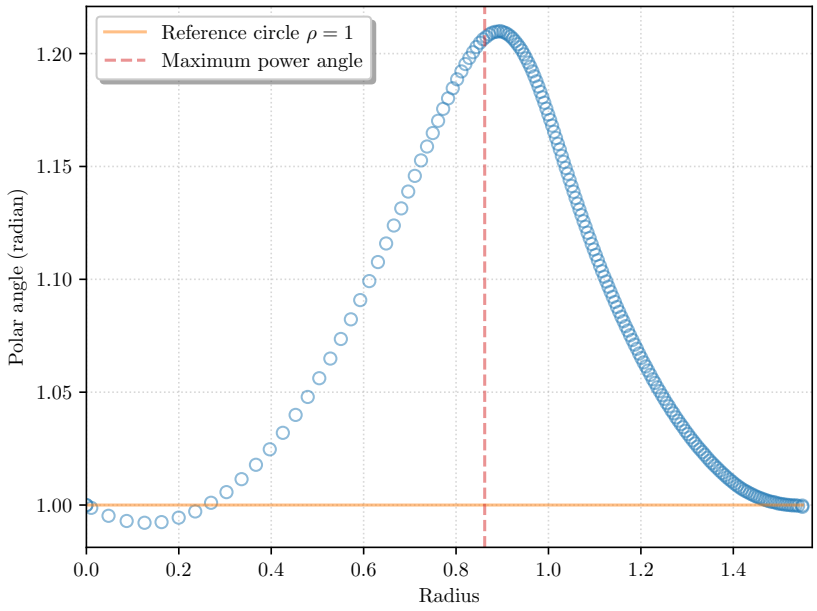

Fig. 3. I–V curve expressed in polar coordinates.

The next property holds for the polar SDM:

Proposition 1. *Let the SDM be expressed in polar coordinates* (ρ, φ)*, denominated polar SDM, where all five scaled parameters* $\{i_{\mathrm{ph}}, i_{\mathrm{o}}, a, r_{\mathrm{s}}, g_{\mathrm{sh}}\}$ *are strictly positive. Then, the slope of the polar SDM is negative at* $\varphi = 0$ *and positive at* $\varphi = \pi/2$*.*

Proof. Let express the SDM as indicated by (7). The total derivative of the radius, ρ, with respect to the angle, φ, is expressed as

$$\frac{\mathrm{d}\rho}{\mathrm{d}\varphi} \coloneqq -\frac{\partial f_{\text{polar}}/\partial\varphi}{\partial f_{\text{polar}}/\partial\rho}, \tag{8}$$

$$\frac{\partial f_{\text{polar}}}{\partial\varphi} = \frac{\rho i_{\text{o}}}{a}\left(r_{\text{s}}\cos(\varphi) - \sin(\varphi)\right)\exp\left(\frac{\rho\left(r_{\text{s}}\sin(\varphi) + \cos(\varphi)\right)}{a}\right) + \rho\left(\left(g_{\text{sh}}r_{\text{s}} + 1\right)\cos(\varphi) - g_{\text{sh}}\sin(\varphi)\right), \tag{9}$$

$$\frac{\partial f_{\text{polar}}}{\partial\rho} = \frac{i_{\text{o}}}{a}\left(r_{\text{s}}\sin(\varphi) + \cos(\varphi)\right)\exp\left(\frac{\rho\left(r_{\text{s}}\sin(\varphi) + \cos(\varphi)\right)}{a}\right) + g_{\text{sh}}\cos(\varphi) + \left(g_{\text{sh}}r_{\text{s}} + 1\right)\sin(\varphi). \tag{10}$$

It can be easily appreciated that $\partial f_{\text{polar}}/\partial\rho \neq 0$ for $\varphi \in [0, \pi/2]$, therefore, according to the implicit function theorem, $\mathrm{d}\rho/\mathrm{d}\varphi$ must exists. Then, evaluating the derivative in the extreme pair of values $(1,\ 0)$ and $(1,\ \pi/2)$, we have:

$$\left(\frac{\mathrm{d}\rho}{\mathrm{d}\varphi}\right)\Big|_{(1,\,0)} = -\frac{\rho\left(i_{\text{o}}r_{\text{s}}\exp\left(\frac{\rho}{a}\right) + a g_{\text{sh}}r_{\text{s}} + a\right)}{i_{\text{o}}\exp\left(\frac{\rho}{a}\right) + a g_{\text{sh}}}, \tag{11}$$

$$\left(\frac{\mathrm{d}\rho}{\mathrm{d}\varphi}\right)\Big|_{(1,\,\pi/2)} = \frac{\rho\left(i_{\text{o}}\exp\left(\frac{\rho}{a}\right) + a g_{\text{sh}}\right)}{i_{\text{o}}r_{\text{s}}\exp\left(\frac{\rho}{a}\right) + a g_{\text{sh}}r_{\text{s}} + a}, \tag{12}$$

$$\tag{13}$$

then, $\left(\mathrm{d}\rho/\mathrm{d}\varphi\right)\big|_{(1,\,0)} < 0$ and $\left(\mathrm{d}\rho/\mathrm{d}\varphi\right)\big|_{(1,\,\pi/2)} > 0$ ∎

III. Cost functions

Next, the five used cost functions are described in detail.

A. *PV current RMSD*

The optimal value of n is computed based on the current root mean squared deviation (RMSD):

$$\min \sum_{j=1}^{n} (I_{\mathrm{m},j} - I_{\mathrm{k},j})^2, \tag{14}$$

where every current I is computed for the same input voltage. In this formulation, the voltage is an input. This function has been found in [7].

B. *Functional RMSD*

The functional RMSD takes advantage of (2),

$$\min \sum_{j=1}^{n} f_{\mathrm{sd},j}^2. \tag{15}$$

Here, the current and the voltage are inputs. This function has been found in [8].

C. *Area difference*

This method computes the area of the difference

$$\Delta I = |I_{\mathrm{m}} - I_{\mathrm{k}}|, \tag{16}$$

where it is minimized

$$\min \sum_{j=1}^{n-1} \left|V_{\mathrm{m},j+1} - V_{\mathrm{m},j}\right| \left(\Delta I_j + \Delta I_{j+1}\right) \tag{17}$$

In this approach, the absolute value is incorporated for not depending on the order of the voltage input (increasing or decreasing.) This method was presented in [9].

D. *Orthogonal distance regression*

The orthogonal distance regression (ODR) attempts to minimize the orthogonal distance of all points between the measurement and the estimation. Fig. 4 indicates the orthogonal distance 'd' for two cases. Then, the ODR aims to minimize [10]

$$\min \sum_{j=1}^{n} \left(\frac{V_{\mathrm{m},j} - V_{\mathrm{k},j}}{\sigma_v} \right)^2 + \left(\frac{I_{\mathrm{m},j} - I_{\mathrm{k},j}}{\sigma_i} \right)^2 . \tag{18}$$

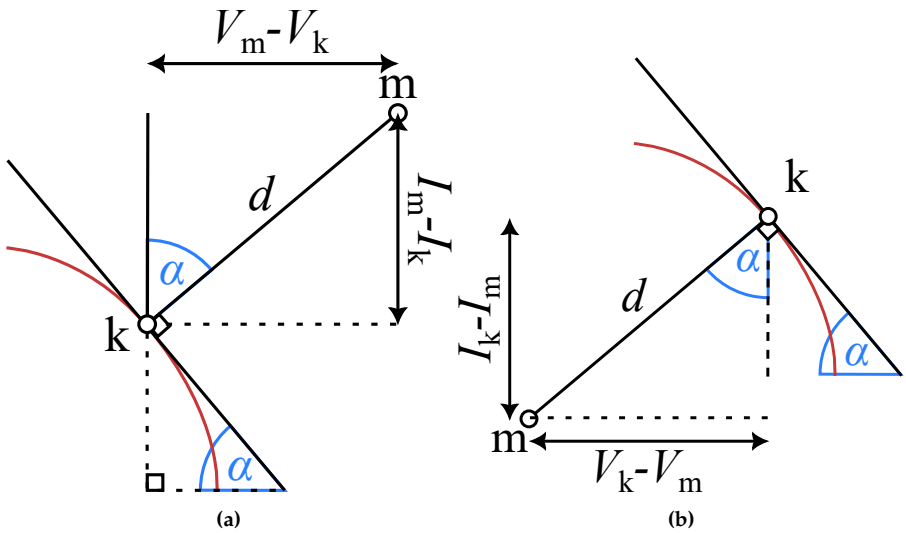

Fig. 4. Orthogonal distance between a measured point 'm' and an estimated point 'k' which belongs to the model. Panel (a) and (b) depicts the two possible scenarios. Left panel adapted from [10].

The estimation of the point kk can be performed using the procedure described by Batzelis *et al.* [10]. Since the set of points kk must be estimated each time the cost function is invoked, the ODR is more computationally demanding and, consequently, slower. However, as noted in [10], the ODR is presented as a method which maximizes the likelihood of the estimation.

E. *Polar RMSD*

The polar RMSD used the same mathematical structure as the PV current RMSD:

$$\min \sum_{j=1}^{n} \left(\rho_{\mathrm{m},j} - \rho_{\mathrm{k},j} \right)^2 . \tag{19}$$

Here, the radius can be computed explicitly from the measured angle φ_{m} by using the LambertW function.

IV. Results and discussion

A. *Synthetic data analysis*

The synthetic data is generated using the one-dimensional single-diode model. Two set I–V curves are considered: noise free and noisy curve. The former, uses as basis the noise free I–V pairs, $(V_{\mathrm{nf}},\, I_{\mathrm{nf}})$, but incorporates normally distributed noise on the voltage and current as:

$$V_{\mathrm{nn},\,j} = \mathcal{N}\left(V_{\mathrm{nf},\,j},\, \sigma^2_{V_{\mathrm{oc}},\,j}\right) \quad \text{for } j \in 1..n_{\mathrm{data}}, \tag{20}$$

$$I_{\mathrm{nn},\,j} = \mathcal{N}\left(I_{\mathrm{nf},\,j},\, \sigma^2_{I_{\mathrm{sc}},\,j}\right) \quad \text{for } j \in 1..n_{\mathrm{data}}, \tag{21}$$

where $(V_{\mathrm{nn}},\, I_{\mathrm{nn}})$ represents the noisy pairs of voltage and current, and σ indicates the standard deviation. The base parameters used in the generation of data are indicated in Table 1. The file Cocoa_mSi460A8 from the NREL dataset [1] is used as basis for computing the SDM-1 (assuming $n = 1$.)

Table 1. Parameters' value used in the generation of the synthetic data. Every displayed parameter correspond to the mean value of the input data corresponding to the file Cocoa_mSi460A8 from [1], in the range 950 $\mathrm{W\,m^{-2}}$ to 1 050 $\mathrm{W\,m^{-2}}$. The number of solar cells of this module corresponds to 36.

Parameter	Mean value
E_{poa} ($\mathrm{W\,m^{-2}}$)	998.47
T_{mod} (°C)	45.84
I_{sc} (A)	4.98
V_{mp} (V)	15.72
I_{mp} (A)	4.55
V_{oc} (V)	20.10
σ_v (V)	0.11
σ_i (A)	0.02

The generated I–V curves are depicted by Fig. 5. These I–V curves are computed starting from an evenly voltage distribution. In consequence, the I–V curve expressed in polar coordinates is not evenly spaced. This can be improved if an interpolation on φ is performed. However, in this work, we will perform the optimization using the original data pairs.

The cost functions for the noisy and noise free data are presented in Fig. 6. It is appreciated in Fig. 6(a) that the minimum value of every cost function is located at $n = 1$. However, the rate of change at which every function reach that minimum is different. On the other hand, when noise is incorporated into the measurements, it can be seen that the minimum of the functions is no longer located at $n = 1$ (see Fig. 6(b)). This fact suggest that not all the cost function deal in the same way with noise. Moreover, the functional approach is the most impacted approach, modifying its minimum value from 1 to 1.41 (see Table 2).

From Table 2, it is evident that the polar RMSD can accurately reproduce the non-ideal factor of the diode even in the presence of noise. Additionally, this

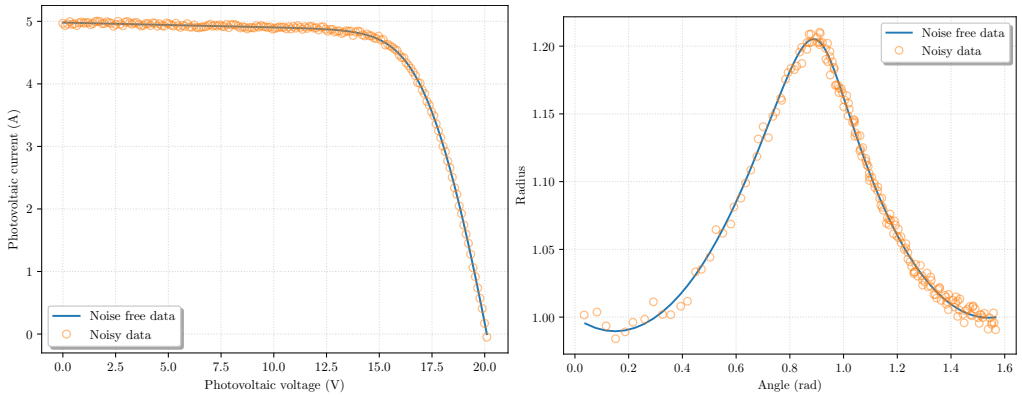

(a) **(b)**

Fig. 5. Synthetic pairs of I–V curves generated from an evenly voltage distribution within the range $[0, V_{oc}]$. Here, the blue curve indicates the noise free pairs while the orange dots indicates the normally distributed noise pairs. Panel (a) shows the I–V curve while panel (b) indicates the I–V curve expressed in polar coordinates.

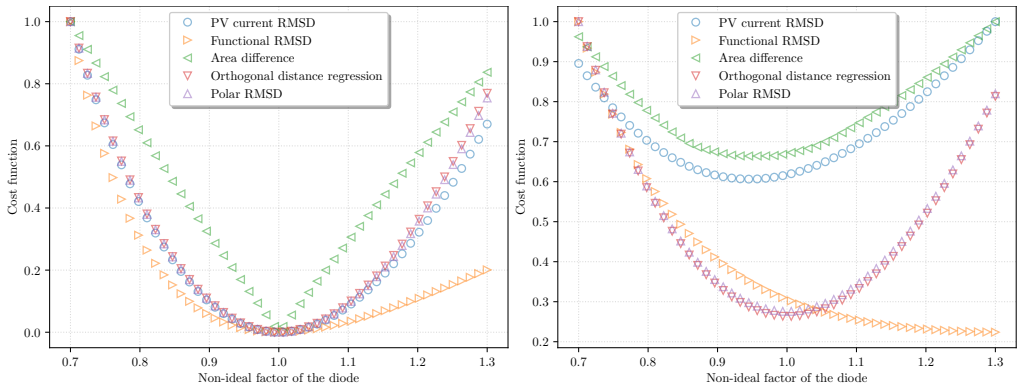

(a) **(b)**

Fig. 6. Scaled cost functions according to its maximum value. Panel (a) shows the noise free scenario, and panel (b) shows the normally distributed noise scenario.

table shows that the ODR has the longest execution time due to its higher computational demand compared to the other methods. This difference is significant, with a difference of two orders of magnitude—ranging from 1 to 1×10^{-2}. As for the computational speed of the polar approach, it is comparable to that of the PV current RMSD since both are computed in a similar manner.

Table 2. Summary of the optimal non-ideal factor of the diodes and execution times obtained for all five cost functions.

Method	Optimal n	Execution time (s)
PV current RMSD	0.95	4.69×10^{-2}
Functional RMSD	1.41	1.56×10^{-2}
Area difference	0.94	7.81×10^{-2}
Orthogonal distance regression	0.94	1.50
Polar RMSD	1.00	3.12×10^{-2}

B. Application to the NREL data set

The Cocoa_mSi460A8 solar module is used as the basis for this analysis. Data within the irradiance range of 950 W m^{-2} to 1 050 W m^{-2} was utilized, resulting in 3,924 I–V curves for examination. Fig. 7 displays a sample I–V curve along with the optimal curves obtained from the five different methods. The similarity between the optimal I–V curves produced by the polar approach and the ODR suggests that their cost functions yield comparable optimal values, as indicated in Table 3. It can be observed from Fig. 7(b) that the polar approach tends to reduce the error in the voltage range from 0 to V_{mp} while increasing it in the range from V_{mp} to V_{oc}. This effect is due to the non-linear nature of the I–V curve.

Table 3. Summary of the optimal non-ideal factor of the diodes and execution times obtained for all five cost functions. The I–V curve used as basis is depicted in Fig. 7.

Method	Optimal n	Execution time (s)
PV current RMSD	1.30	4.69×10^{-2}
Functional RMSD	1.33	4.69×10^{-2}
Area difference	1.25	1.09×10^{-2}
Orthogonal distance regression	1.25	1.06
Polar RMSD	1.20	4.69×10^{-2}

Fig. 8 presents a boxplot of the diode's non-ideal factor n and the execution

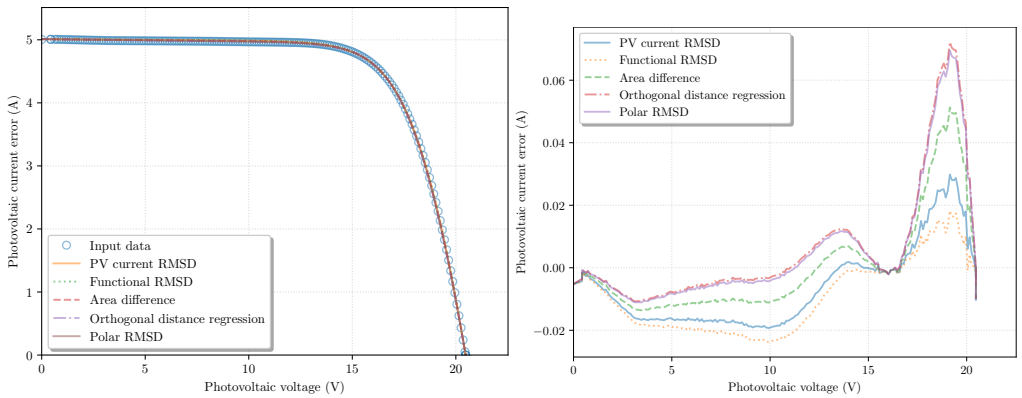

Fig. 7. Optimal I–V curves computed by using the five methods. Panel (a) shows curves in the voltage range from 0 to V_{mp}, while panel (b) completes the I–V curve presenting the voltage range from V_{mp} to V_{oc}. The presented I–V curve corresponds to a random sample of the solar module Cocoa_mSi460A8 in the range 950 W m^{-2} to 1 050 W m^{-2} [1].

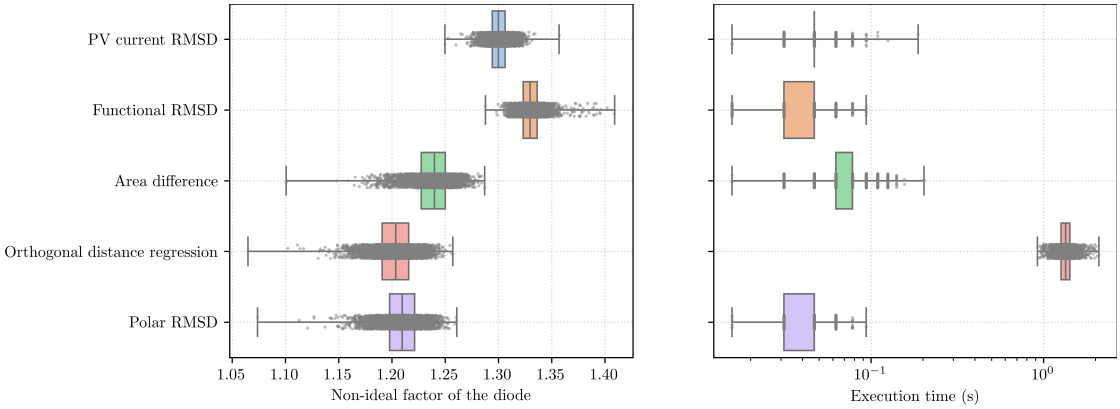

Fig. 8. Boxplot presented for the non-ideal factor of the diode and the execution time. The presented I–V curve corresponds to a random sample of the solar module Cocoa_mSi460A8 in the range 950 W m^{-2} to 1 050 W m^{-2} [1].

times. It can be observed that the optimal n values for the area difference, ODR, and polar RMSD methods are similar, falling approximately within the range of 1.1 to 1.25. In contrast, the PV current RMSD and functional RMSD methods tend to predict higher n values, leading to greater deviations in the voltage region [0, V_{mp}] (see Fig. 7(a)).

Acknowledgments

The work of D. Dutykh has been supported by the French National Research Agency, through the Investments for Future Program (ref. ANR-18-EURE-0016 - Solar Academy). In addition, C. Cárdenas-Bravo would like to acknowledge the INES.2S French Institute for the Energy Transition, the PhD's contract USMB/2021-454, and the CSMB — Conseil Savoie Mont Blanc for its support. This publication is based upon work supported by the Khalifa University of Science and Technology under Award No. FSU-2023-014.

References

[1] W. Marion, A. Anderberg, C. Deline, S. Glick, M. Muller, G. Perrin, J. Rodriguez, S. Rummel, K. Terwilliger, and T. J. Silverman, "User's Manual for Data for Validating Models for PV Module Performance," National Renewable Energy Laboratory (NREL), Technical Report, Apr. 2014.

[2] W. Shockley, *Electrons and Holes in Seminconductors with applications to transistor electronics*. D. Van Nostrand Company, Nov. 1950.

[3] A. Laudani, F. Mancilla-David, F. Riganti-Fulginei, and A. Salvini, "Reduced-form of the photovoltaic five-parameter model for efficient computation of parameters," *Solar Energy*, vol. 97, pp. 122–127, Nov. 2013.

[4] F. J. Toledo, J. M. Blanes, V. Galiano, and A. Laudani, "In-depth analysis of single-diode model parameters from manufacturer's datasheet," *Renewable Energy*, vol. 163, pp. 1370–1384, Jan. 2021.

[5] C. Cárdenas-Bravo, D. Dutykh, and S. Lespinats, "On the parameters domain of the single-diode model," *Solar Energy*, vol. 277, p. 112718, Jul. 2024. [Online]. Available: https://www.sciencedirect.com/science/article/pii/S0038092X24004134

[6] S. Lespinats, A. Revel, and A. Plissonnier, "Procédé et dispositif de diagnostic de fonctionnement d'une chaîne de modules photovoltaïques comprenant au moins un module photovoltaïque," France Patent FR3 130 453A1, Jun., 2023.

[7] T. Easwarakhanthan, J. Bottin, I. Bouhouch, and C. Boutrit, "Nonlinear Minimization Algorithm for Determining the Solar Cell Parameters with Microcomputers," *International Journal of Solar Energy*, vol. 4, no. 1, pp. 1–12, Jan. 1986.

[8] M. F. AlHajri, K. M. El-Naggar, M. R. AlRashidi, and A. K. Al-Othman, "Optimal extraction of solar cell parameters using pattern search," *Renewable Energy*, vol. 44, pp. 238–245, Aug. 2012. [Online]. Available: https://www.sciencedirect.com/science/article/pii/S0960148112000936

[9] B. Arcipiani, "Generalization of the area method for the determination of the parameters of a non-ideal solar cell," *Revue de Physique Appliquée*, vol. 20, no. 5, pp. 269–272, May 1985. [Online]. Available: http://dx.doi.org/10.1051/rphysap:01985002005026900

[10] E. Batzelis, J. M. Blanes, F. J. Toledo, and V. Galiano, "Noise-Scaled Euclidean Distance: A Metric for Maximum Likelihood Estimation of the PV Model Parameters," *IEEE Journal of Photovoltaics*, pp. 1–12, Jan. 2022.